ChemComm
Chemical Communications

Accepted Manuscript

This article can be cited before page numbers have been issued, to do this please use: M. Zhao, L. Cui and C. Zhang, *Chem. Commun.*, 2020, DOI: 10.1039/C9CC09999A.

ROYAL SOCIETY OF CHEMISTRY

rsc.li/chemcomm

ROYAL SOCIETY OF CHEMISTRY View Article Online
DOI: 10.1039/C9CC09999A

Journal Name

COMMUNICATION

Host-guest recognition coupled with triple signal amplification endows electrochemiluminescent biosensor with enhanced sensitivity

Received 00th January 20xx,
Accepted 00th January 20xx

DOI: 10.1039/x0xx00000x

Min-hui Zhao, Lin Cui*, Chun-yang Zhang*

We demonstrate for the first time that the host-guest recognition coupled with triple signal amplification endows the electrochemiluminescent (ECL) biosensor with enhanced sensitivity for uracil DNA glycosylase (UDG) assay. This biosensor exhibits good selectivity and extremely high sensitivity, and it can be used to screen the UDG inhibitors and measure the cellular UDG activity as well.

Metal–organic frameworks (MOFs) are composed of metal clusters/ions which are connected by special organic linkers and exhibit superior physical and chemical properties. Due to the unique properties including big surface areas, large pore volumes, tunable surface chemistry and pore size, multiple topologies, MOFs have functioned as the promising porous materials with wide applications in the adsorption and separation, sensing, catalysis, drug delivery and imaging.[1-5] Prussian blue is identified as one of metal-organic coordination network (MOCN) materials, in which iron ions are bridged by the CN group (-(Fe-CN-Fe)-).[6,7] MOF can be used as the label for the synthesis of prussian blue,[8] and prussian blue possesses low redox potential and high electrocatalytic properties.[9-11]

Electrochemiluminescence (ECL) is an electrochemically triggered optical radiation process produced by the energy relaxation of excited species.[12,13] ECL combines the advantages of luminescence and electrochemical techniques and is becoming an increasingly popular biosensing platform for the detection of metal ions and small molecules as well as the development of ECL immunoassay, ECL genosensors, and ECL cytosensors.[14,15] Especially, ECL not only inherits the characteristics of chemiluminescence (CL) (e.g., high sensitivity and wide dynamic range), but also possesses the advantages of electrochemical methods (e.g., simplicity, stability, and facility).[16-18] Three common types of luminophores including luminol,[19,20] ruthenium (II) complexes,[14] and quantum dots[16] are widely used in ECL studies. Among them, luminol exhibits good chemical stability and low oxidation potential.[19] In addition, a variety of strategies such as the use of horseradish peroxidase[19,21] and DNAzyme[16,22] have been introduced to amplify the ECL signal. However, peroxidase inevitably suffers from the high preparation cost and easy denaturation. Alternatively, prussian blue as a mimic peroxidase can catalyze the oxidation of luminol by the dissolved oxygen to generate an enhanced chemiluminescence signal.[11]

Because the recognition motifs are specific and bioorthogonal, supramolecular noncovalent interaction between host and guest molecules has found wide applications in catalysis[23] and the development of electrochemiluminescent[24] and electrochemical sensors.[25,26] Cyclodextrins (CDs) are one kind of special oligosaccharides with six, seven, and eight glucose units. The unique cage structure endows CDs and their derivatives with excellent recognition and encapsulation capabilities towards the guest molecules, and they may function as the host molecules in biosensors.[24-26] The adsorption of β-CD on the carbon materials (e.g., carbon nanotubes and graphene) can produce water-soluble nanocomposites through hydrogen bonding, van der Waals force, and hydrophobic interaction.[27] Ferrocene (Fc) is a redox molecular, and it can be used for the development of inclusion complexes with β-CD to enhance their solubility, electro-stability and bioavailability.[28] In addition, the electrochemically oxidized Fc (Fc^+) can catalyze the deposition of H_2O_2 to produce $OH^\bullet$ for the generation of an enhanced ECL signal in luminol–H_2O_2 system,[29] meanwhile Fc (Fc^+) exhibits distinct advantages of high stability against various temperature and pH.[30]

In this research, we demonstrate for the first time that the combination of host-guest recognition with triple signal amplification endows the ECL biosensor with enhanced sensitivity for UDG assay. The introduction of prussian blue and Fc on the electrode can catalyze the deposition of H_2O_2 to produce $OH^\bullet$ which may subsequently catalyze the luminol–

College of Chemistry, Chemical Engineering and Materials Science, Collaborative Innovation Center of Functionalized Probes for Chemical Imaging in Universities of Shandong, Key Laboratory of Molecular and Nano Probes, Ministry of Education, Shandong Provincial Key Laboratory of Clean Production of Fine Chemicals, Shandong Normal University, Jinan 250014, China. E-mail: cyzhang@sdnu.edu.cn; zpbzcl@126.com; Fax: +86-531-82615258; Tel: +86-531-86186033

† Electronic Supplementary Information (ESI) available: details of experimental procedures and additional figures. See DOI: 10.1039/x0xx00000x

View Article Online DOI: 10.1039/C9CC09884A

H_2O_2 system to generate an enhanced ECL signal. Moreover, the introduction of supramolecular host–guest interaction between β-CD and Fc greatly simplifies the experimental procedures. Especially, this ECL biosensor involves triple signal amplification and possesses extremely high sensitivity, and it can be further applied for the screening of UDG inhibitors and the measurement of cellular UDG activity.

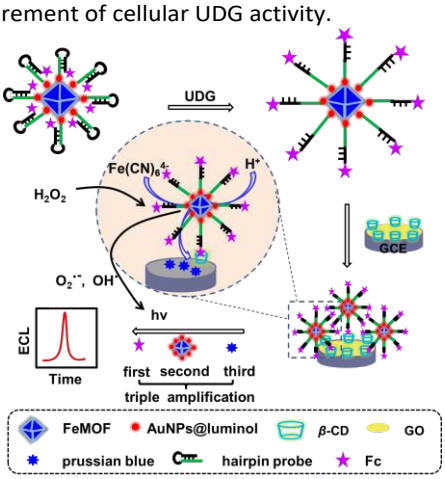

Scheme 1. Schematic representation of the detection of UDG by ECL biosensor via host-guest recognition coupled with triple signal amplification.

Scheme 1 shows the principle of the detection of UDG by ECL biosensor. We designed a hairpin probe with six uracil bases in the stem, whose 3' end is modified with a Fc as the first signal amplification redox and 5' end is modified with a thiol group for immobilization on the FeMOF/AuNPs@luminol as the second signal amplification platform. In the absence of UDG, the six uracil bases in the stem of hairpin probe cannot be removed, and the Fc on the FeMOF/AuNPs@luminol-hairpin probe cannot be captured by β-CD on the GO-modified electrode, leading to no production of prussian blue. As a result, a low ECL is observed due to the absence of Fc and prussian blue on the electrode. In the presence of UDG, it can remove six uracil bases from the hairpin DNA stem to produce six AP sites, generating a ssDNA whose 3' end is modified with Fc. The β-CD on the electrode can recognize Fc via host–guest interaction and subsequently electrochemically oxidized Fc (Fc^+) catalyzes the reaction of luminol radical ($L^{-\bullet}$) with $OH^\bullet$, which is produced from H_2O_2, to form 3-aminophthalate (AP^{2-}*). When AP^{2-}* returns to the ground state, an enhanced ECL signal is generated. Moreover, the addition of acid (H^+) and $K_4Fe(CN)_6$ enables their reaction with Fe^{3+} in FeMOF, resulting in the production of prussian blue ($[Fe^{III}Fe^{II}(CN)_6]^-$). Prussian blue can catalyze the formation of AP^{2-}* in the presence of H_2O_2 in alkaline solution, enabling the third ECL signal amplification.

The generation of an enhanced ECL signal involves following five steps. H_2O_2 induces a one-electron oxidation of luminol monoanion (LH^-) to diazasemiquinone radical ($L^{-\bullet}$) (eq. 1); Diazasemiquinone radical produces $O_2^{\bullet-}$ in the presence of O_2 (eq. 2); electrochemically oxidized Fc (Fc^+) and prussian blue catalyze the deposition of H_2O_2 to produce $OH^\bullet$ (eq. 3, the generation of $OH^\bullet$ is verified by the electron spin resonance (EPR) spectra (see ESI,† Fig. S1));[31] the resultant $O_2^{\bullet-}$ and $OH^\bullet$ radicals react with luminol radical ($L^{-\bullet}$) to form AP^{2-}* (eq. 4); when AP^{2-}* returns to the ground state, an enhanced ECL signal is generated (eq. 5).[32]

$$LH^- - e^- \rightarrow LH^\bullet \rightarrow L^{-\bullet} + H^+ \quad (1)$$

$$L^{-\bullet} + O_2 \rightarrow O_2^{\bullet-} + L \quad (2)$$

$$L^{-\bullet} + H_2O_2 \xrightarrow[\text{prussian blue}]{Fc^+} OH^\bullet + L + H_2O \quad (3)$$

$$L^{-\bullet} \xrightarrow{OH^\bullet\ O_2^{\bullet-}} AP^{2-}* + \text{product} \quad (4)$$

$$AP^{2-}* \longrightarrow AP^{2-} + hv \quad (5)$$

We used XRD pattern to characterize the crystal structure of the obtained FeMOF (Fig. 1A). FeMOF displays main diffraction peaks at 18.88°, 16.46°, 9.98°, and 9.06° (Fig. 1A, curve a), corresponding to the (201), (200), (101), and (002) planes, respectively.[33] We used UV–vis spectra to characterize the AuNPs@luminol (Fig. 1B). The spectrum of luminol exhibits the characteristic peaks at 300 and 360 nm (Fig. 1B, curve a). The spectrum of 13-nm AuNPs shows an absorption peak at 525 nm (Fig. 1B, curve b). In contrast, in the UV–vis spectrum of the AuNPs@luminol colloid, the dual absorption peaks of luminol disappear and two absorption peaks at 368 and 530 nm appear[16] (Fig. 1B, curve c), indicating the formation of luminol-functionalized AuNPs. The high-density luminol on AuNPs is beneficial to the enhancement of anode ECL emission. The morphologies of the AuNPs@luminol, the FeMOF, the FeMOF/AuNPs@luminol, and the obtained prussian blue films are characterized by SEM and TEM, respectively. The typical TEM image of the AuNPs@luminol shows a homogeneous distribution of 20 nm in diameter (Fig. 1C). The SEM image of FeMOF shows the particles with an octahedron morphology and 200 nm in diameter (Fig. 1D). Moreover, Fig. 1E shows the well dispersion of AuNPs@luminol on the FeMOF surface due to electrostatic adsorption between the NH_2 group of FeMOF and the AuNPs@luminol. The measured zeta potential further verifies the adsorption of the AuNPs@luminol on the FeMOF surface, with 17.6 ± 0.4 mV for FeMOF and -25.3 ± 0.3 mV for the AuNPs@luminol, which facilitates their electrostatic interaction to obtain the FeMOF/AuNPs@luminol with a reversed zeta potential of -6.46 ± 0.13 mV. The obtained prussian blue film has porous structure (Fig. 1F) with improved mass-transfer efficiency and large surface area, facilitating the catalyzation of luminol radical to form AP^{2-}* for the generation of an enhanced ECL signal.

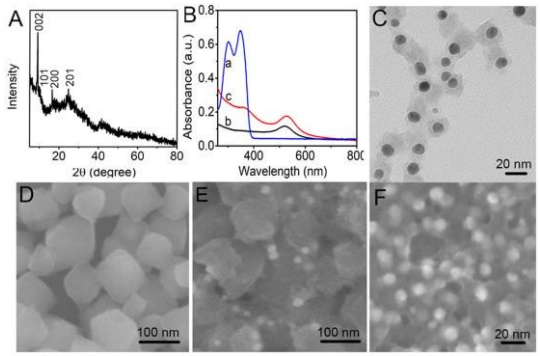

Fig. 1 (A) XRD pattern of FeMOF. (B) UV–vis spectra of luminol (a), AuNPs (b), and the AuNPs@luminol (c). (C) TEM image of the AuNPs@luminol. (D-F) SEM images of FeMOF (D), the FeMOF/AuNPs@luminol (E), and the obtained prussian blue film (F).

In addition, we measured the electrochemical impedance spectra (EIS) of the modified electrodes in different construction steps (see ESI,† Fig. S2A), and experimentally verified that the introduction of prussian blue and Fc onto the electrode can catalyze the deposition of H_2O_2 to produce $OH^{\bullet}$ for the generation of an enhanced ECL signal in the luminol–H_2O_2 system (see ESI,† Fig. S2B).

Under the optimized condition (see ESI,† Fig. S3), the ECL signals generated by various-concentration UDG were measured. As shown in Fig. 2A, ECL signal enhances with the increasing concentration of UDG, with a linear relationship being obtained between the ECL intensity and the logarithm of UDG concentration from 0.0005 to 1 U mL^{-1} (Fig. 2B). The corresponding equation is I_{ECL} = 7422 + 2043 $\log_{10} C$ with a correlation coefficient of 0.9978, where C is the UDG concentration (U mL^{-1}) and I_{ECL} is the measured ECL intensity. The limit of detection (defined by 3 σ/K, where σ is the standard deviation of the blank sample and K is the slope of the linear regression equation) is calculated to be 2.5 × 10^{-4} U mL^{-1}. The sensitivity of the proposed ECL biosensor is much higher than those of the reported methods[34-41] (see ESI,† Table S1), with 3.2-fold higher than that of fluorescent assay,[34-36] 24-fold higher than that of electrochemiluminescent assay,[37] 32-fold higher than that of electrochemical assays,[38-40] 81-fold higher than that of the colorimetric assay.[41] The high sensitivity of the proposed ECL biosensor can be attributed to the involvement of triple signal amplification: (1) the supramolecular host–guest (β-CD–Fc) recognition provides a simple and efficient approach for capturing redox molecule (Fc) whose electrochemically oxidized product (Fc^+) can catalyze the decomposition of H_2O_2 to generate an enhanced ECL signal; (2) each FeMOF carries a large number of AuNPs@luminol-linked hairpin DNAs with abundant luminol molecules which greatly enhance the ECL signal; (3) the reaction of acid (H^+) and $K_4Fe(CN)_6$ with Fe^{3+} in FeMOF results in the production of prussian blue which catalyzes luminol radicals to form AP^{2-*} for the generation of an enhanced ECL signal.

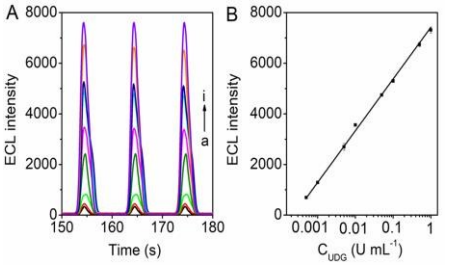

Fig. 2 (A) ECL intensity in response to different concentrations of UDG from a to i: 0, 0.0005, 0.001, 0.005, 0.01, 0.05, 0.1, 0.5, 1 U mL^{-1}. (B) A linear correlation is obtained between the ECL intensity and the logarithm of UDG concentration. Error bars are standard derivation obtained from three independent experiments.

To investigate the selectivity of the proposed ECL biosensor, we used human alkyladenine DNA glycosylase (hAAG), thymine DNA glycosylase (TDG), formamidopyrimidine-DNA glycosylase (FPG), bovine serum albumin (BSA) and immunoglobulin G (IgG) as the interferences. BSA and IgG are not DNA glycosylases, and they cannot remove uracil from the substrates. The hAAG can cleave the alkylated adenine;[42] the FPG can cleave 4,6-diamino-5-formamidopyrimidine, 2,6-diamino-4-hydroxy-5-formamidopyrimidine and 8-hydroxyguanine;[43] TDG can selectively remove T from the G/T mismatches;[44] but none of them can cleave the specific DNA substrate of UDG. Fig. 3A shows that significant ECL enhancement is observed in the presence of UDG. In contrast, no distinct ECL signal is observed in the presence of BSA, hAAG, IgG, FPG, and TDG, respectively, suggesting the proposed ECL biosensor possesses high selectivity towards UDG. Moreover, the proposed ECL biosensor exhibits excellent stability with a relative standard deviation (RSD) of 0.65% for the detection of 1 U mL^{-1} UDG under consecutive cyclic potential scans from 0 to 0.5 V for 12 cycles (Fig. 3B). We further investigated the reproducibility of the proposed ECL biosensor by measuring the same UDG concentration (1 U mL^{-1}) with five electrodes prepared under identical conditions. The RSD was measured to be 2.6%, suggesting good reproducibility of the proposed ECL biosensor.

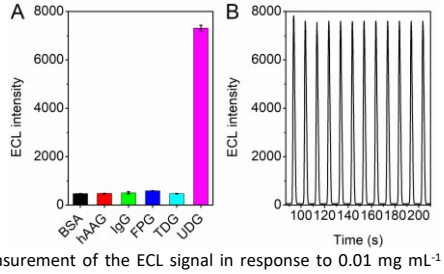

Fig. 3 (A) Measurement of the ECL signal in response to 0.01 mg mL^{-1} BSA, 1 U mL^{-1} hAAG, 0.01 mg mL^{-1} IgG, 1 U mL^{-1} FPG, 1 U mL^{-1} TDG, and 1 U mL^{-1} UDG, respectively. Error bars are standard derivation obtained from three independent experiments. (B) Stability of the proposed ECL biosensor under consecutive cyclic potential scans from 0 to 0.5 V for 12 cycles.

We further demonstrate the feasibility of this ECL biosensor for the detection of UDG activity in HeLa cells. A linear relationship is obtained between the ECL intensity and the logarithm of cell number, and the regression equation is I_{ECL} = 930.9 $\log_{10} N$ − 152.7 with a correlation coefficient of 0.9889, where N is the cell number and I_{ECL} is the measured ECL intensity (Fig. 4). The limit of detection is estimated to be 2 cells, suggesting the high sensitivity of this ECL biosensor for the detection of cellular UDG activity. Moreover, this ECL biosensor can be used for the screening of UDG inhibitors (see ESI,† Fig. S4). In addition, the proposed method can specifically detect UDG in cell lysate without any response to other interferences (see ESI,† Fig. S5), and it can accurately detect UDG spiked in human serum with a recovery rate of 97.0% ± 3.5% ~ 102.0% ± 3.2% (see ESI,† Table S2).

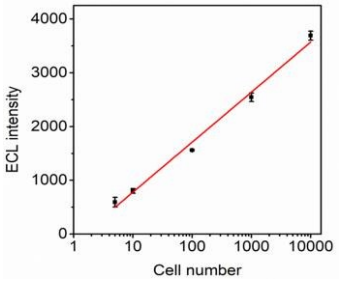

Fig. 4 Linear relationship between ECL intensity and the logarithm of the number of HeLa cells. Error bars are standard derivation obtained from three independent experiments.

In summary, we have demonstrated that the host–guest recognition coupled with triple signal amplification endows the ECL biosensor with enhanced sensitivity for UDG assay. This ECL biosensor involves triple signal amplification including (1) Fc^+ catalyzes the decomposition of H_2O_2 to produce AP^{2-}*; (2) the FeMOF/AuNPs@luminol probe can load abundant luminol molecules to generate an enhanced ECL signal, and (3) prussian blue catalyzes luminol radicals to form AP^{2-}* in the presence of H_2O_2. In addition, the supramolecular host–guest (β-CD–Fc) recognition provides a simple and efficient approach for capturing redox molecule (Fc) whose electrochemically oxidized product (Fc^+) can catalyze the decomposition of H_2O_2 to generate an enhanced ECL signal, greatly simplifying the experimental procedures. Importantly, this ECL biosensor exhibits good selectivity and extremely high sensitivity. It can be further applied for the screening of UDG inhibitors and accurate detection of cellular UDG activity, holding great potential in clinical diagnosis and drug discovery.

This work was supported by the National Natural Science Foundation of China (Grant Nos. 21735003, 21527811, 21605096, and 21974080), and the Award for Team Leader Program of Taishan Scholars of Shandong Province, China.

Conflicts of interest

There are no conflicts to declare.

Notes and references

1. Yang, X.; Yu, Y. Q.; Peng, L. Z.; Lei, Y. M.; Chai, Y. Q.; Yuan, R.; Zhuo, Y. *Anal. Chem.* 2018, **90**, 3995-4002.
2. Xiong, C. Y.; Wang, H. J.; Liang, W. B.; Yuan, Y. L.; Yuan, R.; Chai, Y. Q. *Chem. Eur. J.* 2015, **21**, 9825-9832.
3. Xiong, C.; Liang, W.; Zheng, Y.; Zhuo, Y.; Chai, Y.; Yuan, R. *Anal. Chem.* 2017, **89**, 3222-3227.
4. Jiang, X.; Wang, Z.; Wang, H.; Zhuo, Y.; Yuan, R.; Chai, Y. *Chem. Commun*. 2017, **53**, 9705-9708.
5. Cui, L.; Wu, J.; Li, J.; Ju, H. *Anal. Chem.* 2015, **87**, 10635-10641.
6. Chen, W.; Zeng, K.; Liu, H.; Ouyang, J.; Wang, L.; Liu, Y.; Wang, H.; Deng, L.; Liu, Y. N. *Adv. Funct. Mater.* 2017, **27**, 1605795.
7. Hu, M.; Belik, A. A.; Imura, M.; Mibu, K.; Tsujimoto, Y.; Yamauchi, Y. *Chem. Mater.* 2012, **24**, 2698-2707.
8. Cui, L.; Hu, J.; Li, C. C.; Wang, C. M.; Zhang, C. Y. *Biosens. Bioelectron.* 2018, **122**, 168-174.
9. Zhao, H. X.; Zou, Q.; Sun, S. K.; Yu, C. S.; Zhang, X. j.; Li, R. J.; Fu, Y. Y. *Chem. Sci.* 2016, **7**, 5294-5301.
10. Chen, W. H.; Yu, X.; Cecconello, A.; Sohn, Y. S.; Nechushtai, R.; Willner, I. *Chem. Sci.* 2017, **8**, 5769-5780.
11. Carboni, M.; Abney, C. W.; Liu, S.; Lin, W. *Chem. Sci.* 2013, **4**, 2396-2402.
12. Cai, X. L.; Zheng, B.; Zhou, Y.; Younis, M. R.; Wang, F. B.; Xia, X. H.; Zhang, W. M. *Chem. Sci.* 2018, **9**, 6080-6084.
13. Ma, C.; Wu, W.; Li, L.; Wu, S.; Zhang, J.; Chen, Z.; Zhu, J. J. *Chem. Sci.* 2018, **9**, 6167-6175.
14. Wu, M. S.; Yuan, D. J.; Xu, J. J.; Chen, H. Y. *Chem. Sci.* 2013, **4**, 1182-1188.
15. Zhang, H.; Li, B.; Sun, Z.; Zhou, H.; Zhang, S. *Chem. Sci.* 2017, **8**, 8025-8029.
View Article Online
DOI: 10.1039/C9CC09999A
16. Cheng, Y.; Huang, Y.; Lei, J.; Zhang, L.; Ju, H. *Anal. Chem.* 2014, **86**, 5158-5163.
17. Zhao, M.; Zhuo, Y.; Chai, Y. Q.; Yuan, R. *Biomaterials.* 2015, **52**, 476-483.
18. Liu, Z.; Qi, W.; Xu, G. *Chem. Soc. Rev.* 2015, **44**, 3117-3142.
19. Eßmann, V.; Jambrec, D.; Kuhn, A.; Schuhmann, W. *Electrochem. Commun.* 2015, **50**, 77-80.
20. Sakura, S. *Anal. Chim. Acta.* 1992, **262**, 49-57.
21. Cai, F.; Zhu, Q.; Zhao, K.; Deng, A.; Li, J. *Environ. Sci. Technol.* 2015, **49**, 5013-5020.
22. Huang, Y.; Lei, J.; Cheng, Y.; Ju, H. *Electrochim. Acta.* 2015, **155**, 341-347.
23. Shen, W. J.; Zhuo, Y.; Chai, Y. Q.; Yang, Z. H.; Han, J.; Yuan, R. *ACS Appl. Mater. Interfaces* 2015, **7**, 4127-4134.
24. Gao, J.; Xiong, H.; Zhang, W.; Wang, Y.; Wang, H.; Wen, W.; Zhang, X.; Wang, S. *Carbon.* 2018, **130**, 416-423.
25. Xie, S.; Zhang, J.; Yuan, Y.; Chai, Y.; Yuan, R. *Chem. Commun.* 2015, **51**, 3387-3390.
26. Gao, J.; Guo, Z.; Su, F.; Gao, L.; Pang, X.; Cao, W.; Du, B.; Wei, Q. *Biosens. Bioelectron.* 2015, **63**, 465-471.
27. Guo, Y.; Guo, S.; Ren, J.; Zhai, Y.; Dong, S.; Wang, E. *ACS Nano*, 2010, **4**, 4001-4010.
28. Jiang, J.; Lin, X.; Ding, D.; Diao, G. *Biosens. Bioelectron.* 2018, **114**, 37-43.
29. Wilson, R.; Schiffrin, D. J. *Anal. Chem.* 1996, **68**, 1254-1257.
30. Liu, Y.; Wang, H.; Xiong, C.; Yuan, Y.; Chai, Y.; Yuan, R. *Biosens. Bioelectron.* 2016, **81**, 334-340.
31. Jiang, X.; Chai, Y.; Wang, H.; Yuan, R. *Biosens. Bioelectron.* 2014, **54**, 20-26.
32. Cui, H.; Zou, G. Z.; Lin, X. Q. *Anal. Chem.* 2003, **75**, 324-331.
33. Taylor-Pashow, K. M.; Della Rocca, J.; Xie, Z.; Tran, S.; Lin, W. *J. Am. Chem. Soc.* 2009, **131**, 14261-14263.
34. Jing, T.; Panshu, S.; Yusuke, S.; Seiichi, N.; Norio, T.; Aijun, T.; Yu, X. *Chem. Commun.* 2014, **51**, 929-932.
35. Zhang, L.; Zhao, J.; Jiang, J.; Yu, R. *Chem. Commun.* 2012, **48**, 8820-8822.
36. Zhang, Y.; Li, C. C.; Tang, B.; Zhang, C. Y. *Anal. Chem.* 2017, **89**, 7684-7692.
37. Liu, Q.; Liu, C.; Zhu, G.; Xu, H.; Zhang, X. J.; Hu, C.; Xie, Y.; Zhang, K.; Wang, H. *Microchim. Acta.* 2019, **186**, 179.
38. Liu, X.; Chen, M.; Hou, T.; Wang, X.; Liu, S.; Feng, L. *Electrochim. Acta* 2013, **113**, 514-518.
39. Jiao, F.; Qian, P.; Qin, Y.; Xia, Y.; Deng, C.; Nie, Z. *Talanta* 2016, **147**, 98-102.
40. Zhang, H.; Zhang, L.; Jiang, J.; Yu, R. *Anal. Sci.* 2013, **29**, 193-198.
41. Liu, X.; Chen, M.; Hou, T.; Wang, X.; Liu, S.; Feng, L. I. *Biosens. Bioelectron.* 2014, **54**, 598-602.
42. Wu, Y.; Zhang, B.; Guo, L. H. *Anal. Chem.* 2013, **85**, 6908-6914.
43. Boiteux, S.; Gajewski, E.; Laval, J.; Dizdaroglu, M. *Biochemistry*, 1992, **31**, 106-110.
44. Stivers, J. T.; Jiang, Y. L. *Chem. Rev.* 2003, **103**, 2729-2760.